III. RADIO ASTRONOMY*

Prof. A. H. Barrett	R. J. Allen	M. A. Palfy
Prof. J. W. Graham	R. K. Breon	S. M. Rezende
Prof. M. Loewenthal	Patricia P. Crowther	A. E. E. Rogers
Prof. R. P. Rafuse	A. B. Hull	J. H. Spoor
Dr. D. H. Staelin	W. B. Lenoir	D. H. Steinbrecher
Dr. S. H. Zisk	J. M. Moran, Jr.	A. Vander Vorst

A. MEASUREMENTS OF ATMOSPHERIC ABSORPTION NEAR 1-cm WAVELENGTH

On several days during the summer of 1964, the absorption spectrum of the terrestrial atmosphere was measured at wavelengths near the 1.35-cm water-vapor resonance. These measurements show that the absorption spectrum is related to the water-vapor distribution in the atmosphere. Six of the experiments were accompanied by radiosonde flights launched nearby. These are believed to be the most complete and accurate atmospheric measurements ever made in this spectral region.

The circuit for the Research Laboratory of Electronics five-channel microwave radiometer is shown in Fig. III-1, and is the same system that was used for the

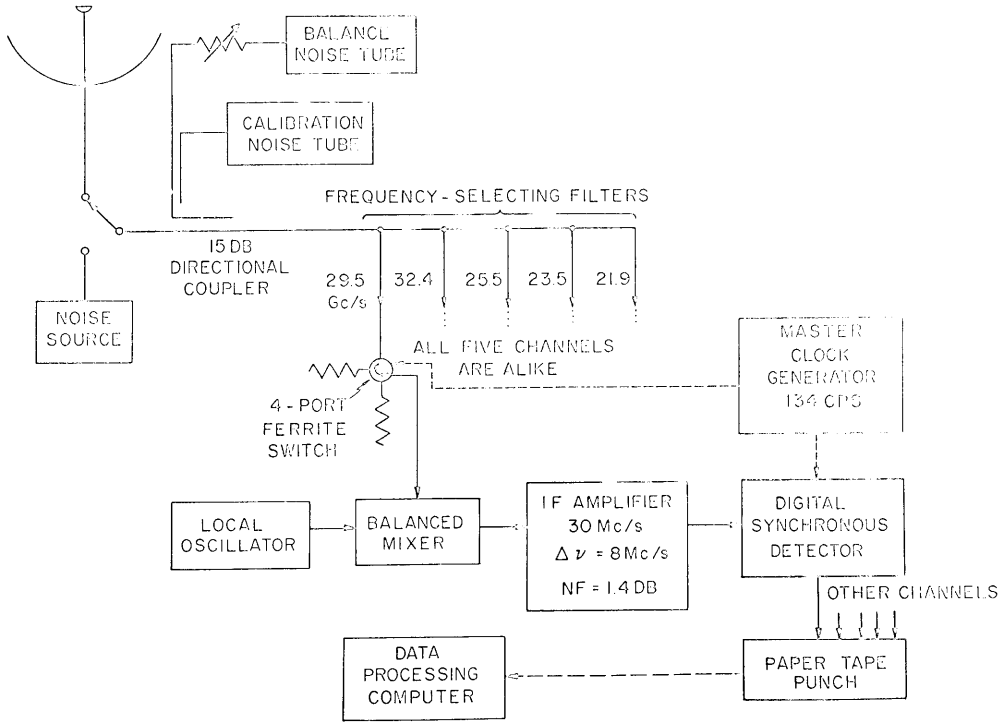

Fig. III-1. Block diagram of the five-channel microwave radiometer.

*This work was supported in part by the National Aeronautics and Space Administration (Grant NsG-419).

1964 observations of Venus.[1] With this radiometer, which was mounted in the 28-ft millimeter wavelength antenna[2] at Lincoln Laboratory, M. I. T., the atmospheric spectra were measured. The frequencies 21.9, 23.5, 25.5, 29.5, and 32.4 Gc/sec were observed simultaneously.

The absorption spectrum was determined by observing the rate of extinction of the solar radiation as the sun set. The curvature of the Earth and the atmospheric refraction did not affect the results because observation at elevation angles below approximately 6° were not incorporated in the data analysis. The results obtained are shown in Table III-1, together with the ground-level humidity measured near sunset.

Table III-1. Measured zenith opacity (db) of the terrestrial atmosphere.

Date	Ground Level H_2O (gm/m^3)	FREQUENCY (Gc/sec)					
		21.0	21.9	23.5	25.5	29.5	32.4
4/21	3.32	.291		.368	.256	.221	.234
5/6	7.00	.309		.380	.247	.184	.208
6/11	6.68		.460	.405	.280	.220	.190
6/12	8.37		.438	.368	.252	.189	.210
8/4(1)	8.05		.545	.484	.330	.224	.222
8/6(2)	7.77		.401	.388	.261	.209	.221
8/7(1)	11.5		.725	.625	.388	.302	.297
8/10(1)	9.18		.713	.687	.409	.282	.318
8/13(2)	7.80		.396	.378	.274	.210	.224
8/14(1)	7.40		.448	.420	.288	.208	.229

(1) The experiment was simultaneous with a radiosonde launched from Cambridge, Massachusetts.

(2) The experiment was simultaneous with a radiosonde launched from Bedford, Massachusetts.

Typical spectra are plotted in Fig. III-2, and the corresponding humidity profiles measured by radiosonde are shown in Fig. III-3. These examples show not only that the microwave spectrum is related to the integrated amount of water vapor in the atmosphere, but also that more sharply peaked spectra indicate larger amounts of water vapor

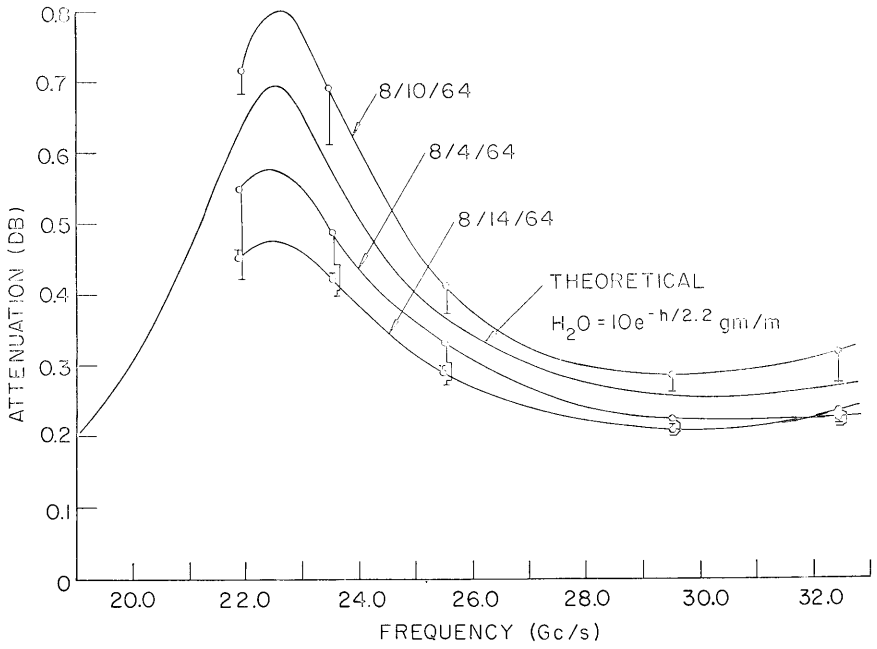

Fig. III-2. Experimental and theoretical zenith opacity of the terrestrial atmosphere. Dots represent experimental values, with an rms uncertainty of approximately ±0.01 db; bars represent the corresponding theoretical values computed from the radiosonde data.

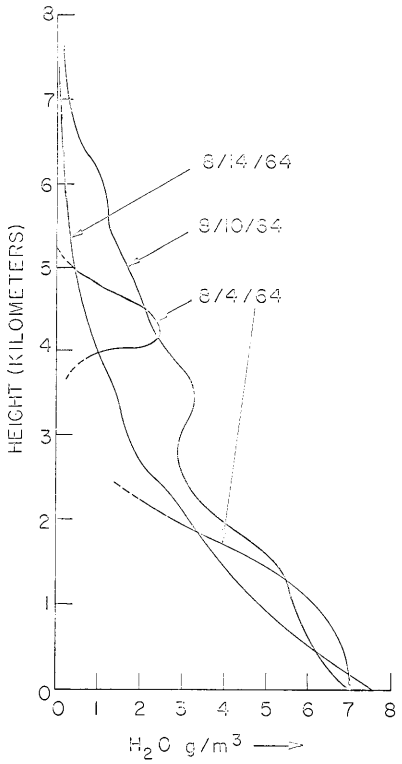

Fig. III-3. Atmospheric water-vapor distribution, as measured by radiosondes launched from the M. I. T. Campus in Cambridge, Massachusetts.

at high altitudes, where the pressure broadening of the resonance is less. Figure III-2 also shows the atmospheric absorption spectra which are computed to correspond to the radiosonde data. The discrepancies are probably due to atmospheric differences between the radiosonde flight path, and the different radiometrically observed regions. The discrepancies may also be due in part to the inaccuracies inherent in radiosondes at high altitudes. Microwave spectral measurements such as these are potentially very useful probes for studying atmospheric water vapor.

D. H. Staelin, A. H. Barrett

References

1. D. H. Staelin and A. H. Barrett, Quarterly Progress Report No. 77, Research Laboratory of Electronics, M. I. T., April 15, 1965, pp. 17-20.
2. D. H. Staelin, Quarterly Progress Report No. 69, Research Laboratory of Electronics, M. I. T., April 15, 1963, pp. 23-25.

B. MEASUREMENT OF ATMOSPHERIC WATER VAPOR AND CLOUDS BY MICROWAVE RADIOMETERS

Ground-based measurements of the microwave spectrum of the terrestrial atmosphere can yield the optical depth, τ, as a function of frequency. These measured values of τ can be used to estimate the integrated water-vapor content of the atmosphere and the integrated cloud content. The water-vapor profile of the atmosphere can also be estimated. Each spectral measurement yields $\tau(\nu_i)$, $i = 1, N$. The problem is to use the measured set of τ_i to estimate $\rho_{H_2O}(h)$. Let $\tau(\nu_i) = \tau_{wv}(\nu_i) + \tau_{cloud}(\nu_i) + \tau_{O_2}(\nu_i)$, where $\tau_{O_2}(\nu_1)$ is known approximately, and $\tau_{cloud}(\nu_i)$ can be determined as shown below.

The function $\tau_{wv}(\nu)$, which is due to water vapor alone, can be expressed as

$$\tau_{wv}(\nu) = \int_{h=0}^{\infty} \alpha(h)\, dh \triangleq \int_{h=0}^{\infty} \rho_{H_2O}(h)\, W(\nu, h)\, dh,$$

where $\alpha(h)$ is the opacity (nepers/m) as a function of height (meters), ρ_{H_2O} is the water-vapor density (gm/m^3), and $W(\nu, h)$ is called the weighting function. $W(\nu, h)$ is a function of both $\rho(h)$ and $T(h)$ (°K), but varies only approximately 1% for typical uncertainties in $\rho(h)$, and approximately 2% for uncertainties in $T(h)$ of 5°K.

If we let

$$\rho_{H_2O}(h) = \sum_{j=1}^{N} \rho_j a_j(h),$$

then

$$\tau_{wv}(\nu_i) = \int_0^\infty \sum_{j=1}^{M} \rho_j a_j(h)\, W(\nu_i, h)\, dh = \sum_{j=1}^{M} W_{ij}\rho_j.$$

Thus

$$[\rho_j] = [W_{ij}]^{-1}\, [\tau_{wv}(\nu_i)].$$

The number of independent parameters ρ_j that can successfully be obtained depends on the number of independent parameters that can be sampled by the $W(\nu_i, h)$, the noise inherent in the measurements of τ, and in the assumption that $W(\nu_i, h)$ is known exactly. In Fig. III-4 several weighting functions $W(\nu, h)$ are plotted. It can be seen

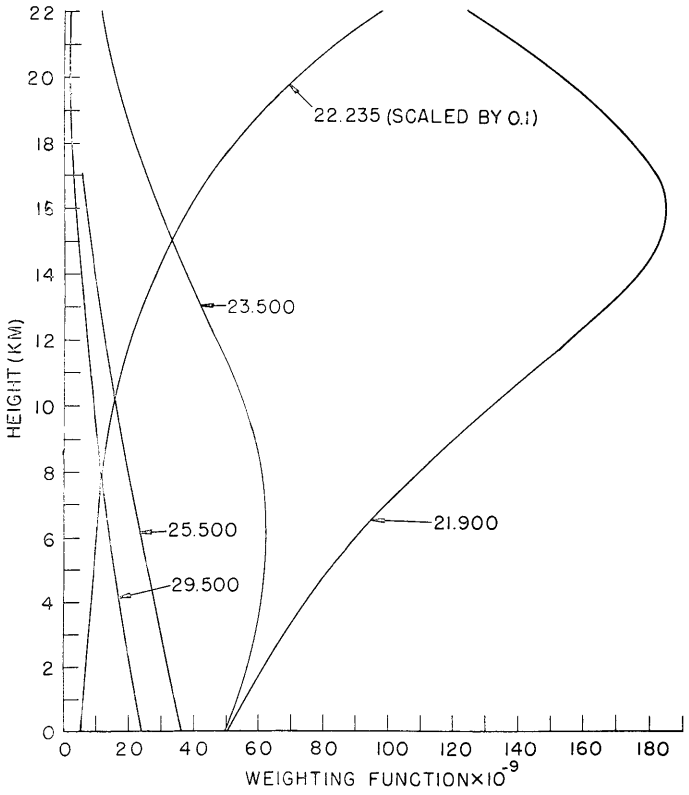

Fig. III-4. Weighting function, $W(\nu, h)$, for atmospheric water vapor.

that near the resonance, 22.235 Gc/sec, the weighting function peaks strongly at high altitudes, whereas at frequencies in the wings of the resonance line the weighting function decreases at high altitudes.

Almost all atmospheric water vapor is below altitude 8 km. Below altitude 8 km the weighting functions are nearly linear; therefore, in this region the space of $W(\nu, h)$ is very nearly spanned by two functions such as $W(22.2, h)$ and $W(25.5, h)$. Consequently, obtaining more than two independent ρ_j for this region would be difficult in the presence of the errors mentioned before. Of course, if there is water vapor above 8 km, additional independent ρ_j could be determined.

The cloud content of the atmosphere may also be determined from measurements of $\tau(\nu)$, and may be determined almost independently of the distribution of atmospheric water vapor.

The absorption coefficient of water clouds in the microwave region 0.5-10 cm is very nearly

$$\alpha_c = \frac{1.01 \times 10^{-6}\ M}{\lambda^2},$$

where M is condensed water (gm/m^3), and λ is wavelength (cm), as given by Goldstein.[1] This is for a cloud temperature of 18°K, and the absorption coefficient varies with temperature approximately 14% at all frequencies for a change of 5°K. The total atmospheric opacity is, then,

$$\tau(\nu_i) = \int_0^\infty \rho_{H_2O}(h)\, W(\nu_i, h)\, dh + k_i H + \tau_{o_2}(\nu_i)$$

$$= A + k_i H + \tau_{o_2}(\nu_i),$$

where k_i and $\tau_{o_i}(\nu_i)$ are known constants except for some uncertainty caused by the temperature uncertainty, and H is the integrated condensed water (gm/cm^2).

Suppose τ is measured at two frequencies, with $W(\nu_1, h) = kW(\nu_2, h)$. For example, 19.0 Gc/sec and 32.4 Gc/sec are such frequencies, and better pairs exist.

Then

$$\tau(\nu_1) - \tau_{o_2}(\nu_1) = kA + k_1 H$$

$$\tau(\nu_2) - \tau_{o_2}(\nu_2) = A + k_2 H.$$

Therefore

$$H = \frac{\tau(\nu_1) - \tau_{o_2}(\nu_1) - k\left(\tau(\nu_2) - \tau_{o_2}(\nu_2)\right)}{k_1 - kk_2}.$$

independently of the distribution of atmospheric water vapor. Of course, the frequencies ν_1 and ν_2 must be such that $k_1 \neq kk_2$. The largest source of error for heavy clouds is

the temperature dependence of the absorption; for light clouds, the errors in $\tau(\nu_i)$.

These same spectral features of clouds and water vapor could be measured from satellites over the ocean, although the equations of radiative transfer introduce an additional dependence on temperature. The error introduced by this dependence should normally be less than approximately 10%, and would partially cancel the errors arising from the temperature dependences of the cloud and water-vapor absorption coefficients.

D. H. Staelin

References

1. H. Goldstein, Propagation of Short Radio Waves, edited by D. E. Kerr (McGraw-Hill Book Company, New York, 1951), p. 676.

C. OBSERVATIONS AT THE HAYSTACK RESEARCH FACILITY

1. Introduction

The Radio Astronomy Group has been conducting radio-astronomical investigations at the Haystack Research Facility of Lincoln Laboratory, M. I. T., located in Tyngsboro, Massachusetts. The antenna is an altazimuth 120-ft paraboloid operating within a 150-ft diameter radome as shown in Fig. III-5. Coupled to the antenna is a Univac U-490 computer that controls the pointing of the antenna and also does preliminary processing of the radiometer data, on a time-sharing basis. At present, two radiometers are available for 3.8-cm and 2-cm wavelengths.

The antenna beamwidth to half-power is 2.3' at 2-cm wavelength, and 4.3' at 3.75 cm, as shown in the diagrams of Fig. III-6. The efficiencies of the antennas were predicted to be 32% and 40%, respectively, but, apparently because of losses in the feed systems, the realized efficiencies were only 15% and 25%. Improved antenna feeds are now under construction.

The antenna follows the altitude and azimuth commands from the computer with a precision of ±0.005° (±20") peak. The computer can generate tracking commands for most of the major bodies of the Solar System, and sidereal tracking for any point in the sky. (The complete repertoire of the pointing program includes a number of other modes with which we are not, for the present, concerned.) Also, the beam can be offset from, or scanned over, the point being tracked in a variety of directions and patterns. This capability facilitates the investigation of fine structure of radio sources.

A more complete description of the Haystack facility has been given elsewhere.[1-3]

2. Radiometric System

The radiometric system was designed by Dr. Sander Weinreb of Lincoln Laboratory, M. I. T., and built under his direction. Radiometers at 8.0 and 15.5 Gc/sec are now

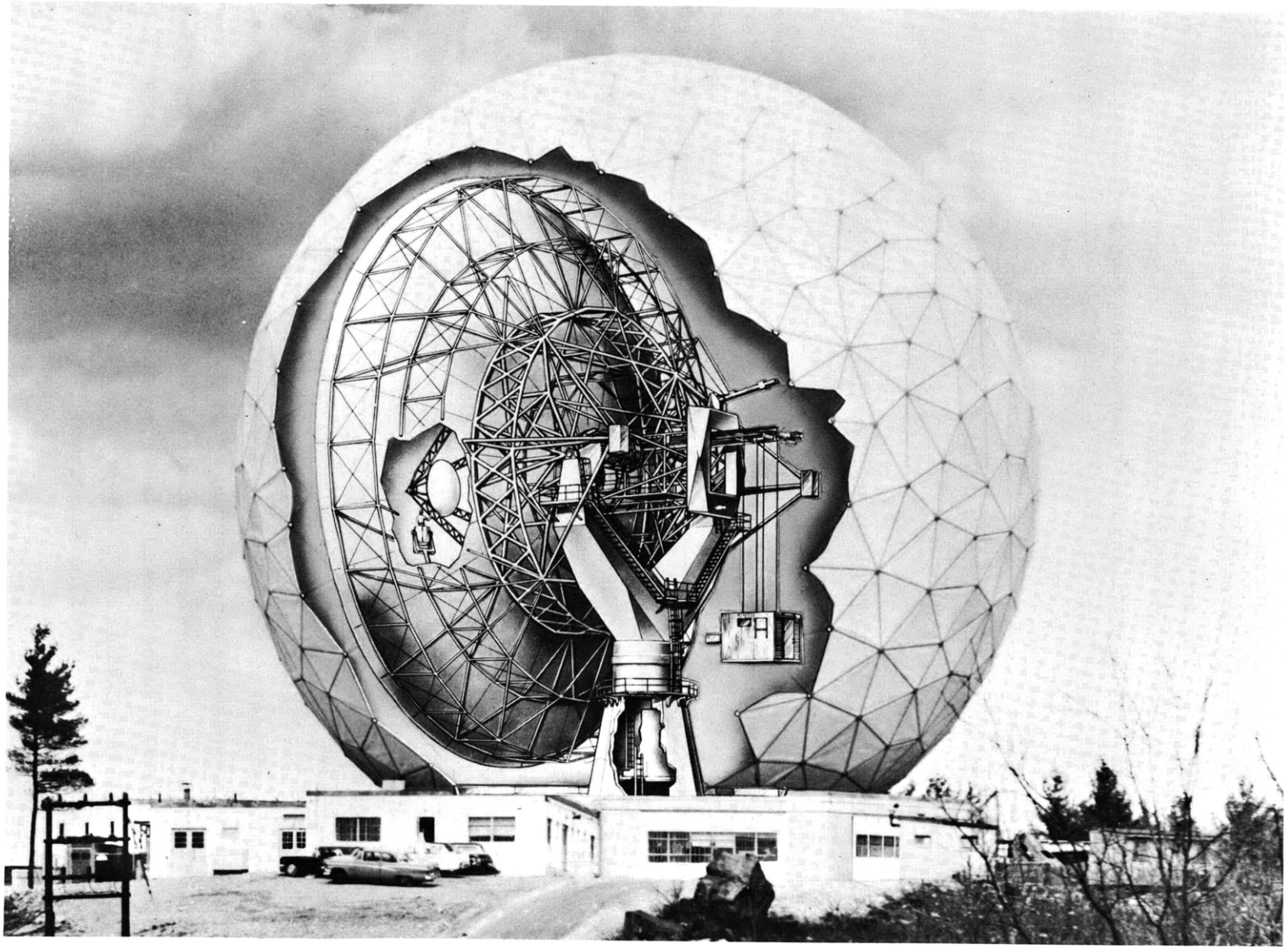

Fig. III-5. Cutaway view of the Haystack Research Facility.

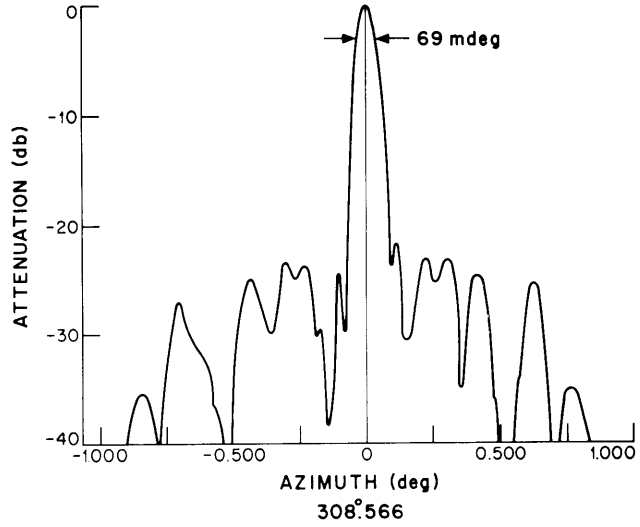

(a)

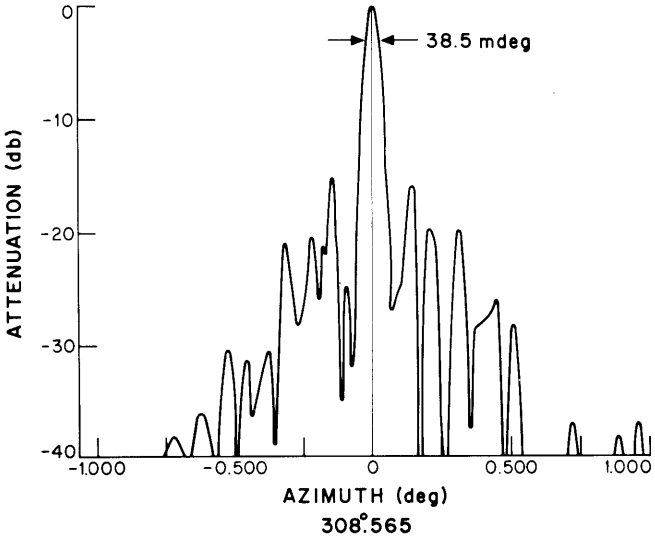

(b)

Fig. III-6. Cross sections of the beam patterns of the Haystack antenna in azimuth (a) 7. 750 Gc/sec, and (b) 15. 745 Gc/sec.

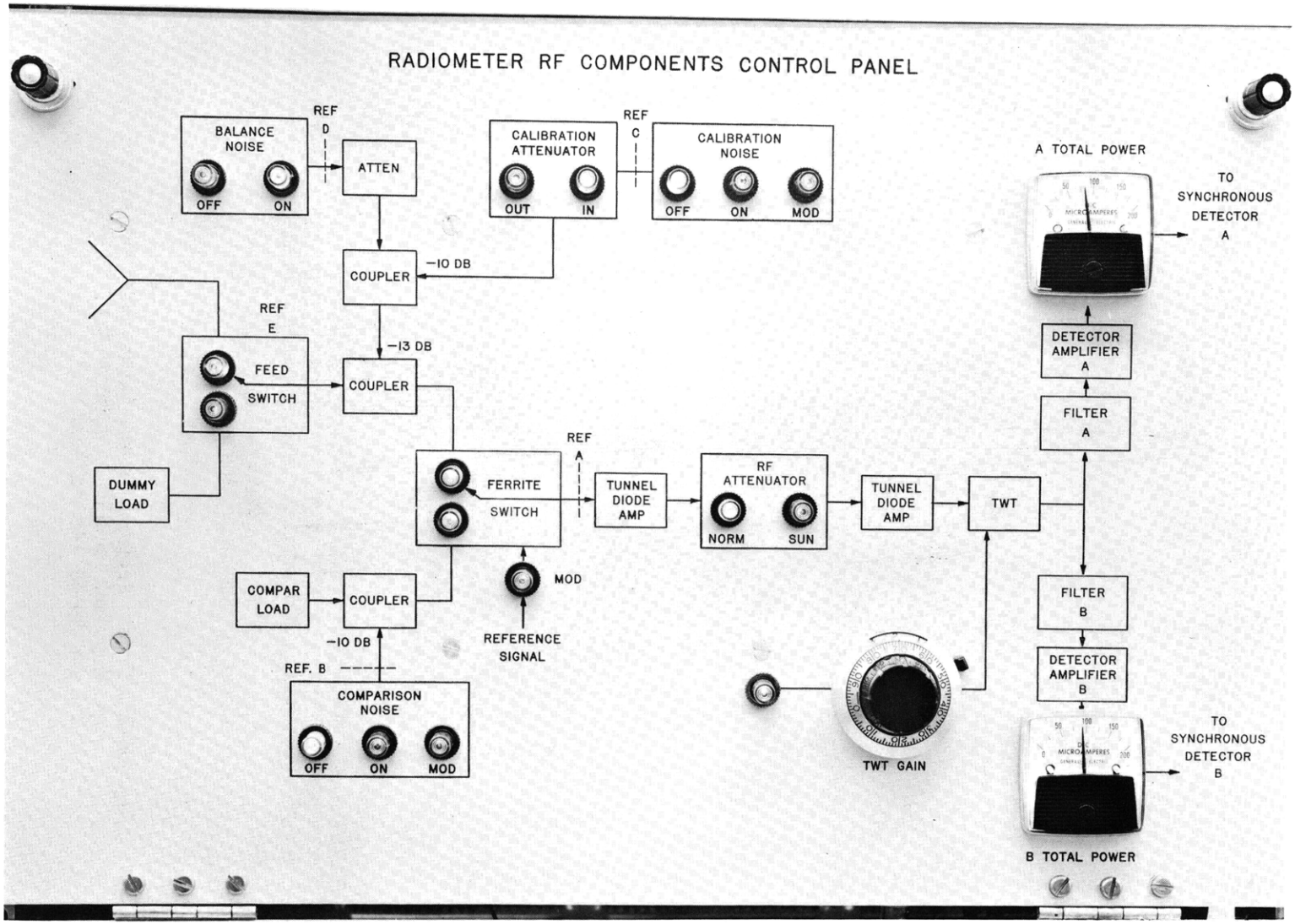

Fig. III-7. Receiver control panel, showing a block diagram of the radiometer.

operational, and a 5.0-Gc/sec radiometer is under construction. These three radiometers are all of the same design, employing a 40-cps ferrite switch on the front end. The system may be connected in the conventional Dicke configuration with the antenna on one side of the switch and a room-temperature load on the other. It is also possible to connect an off-axis feed horn to the comparison side of the input switch in a beam-switching configuration. Tunnel diode devices are used as RF amplifiers, having a bandwidth of 100 Mc/sec. Despite their high noise temperature, the stability, simplicity, and reliability of these devices have made them most satisfactory. A travelling-wave tube is used to provide enough input to properly drive the detectors. After the TWT the passband is split into two 500-Mc/sec segments (to help detect interference) and then into separate precision square-law detectors. The signal in each of these two channels is then processed in a synchronous detector and linear integrator, also designed by Dr. Weinreb, for use with the digital interface directly to the U-490 computer. A block diagram of the radiometers is shown in Fig. III-7. Radiometers for the hydrogen line (1.42 Gc/sec), OH line (1.67 Gc/sec) and 35 Gc/sec are also under construction. Measured and expected operating parameters are tabulated below.

Frequency (Gc/sec)	Noise Temperature (°K)	Bandwidth (Mc/sec)	$(\Delta T)_{rms}$ (°K)	Construction Status
1.42	250	10	0.05	design stage
1.67	120	10	0.02	under construction
5.0	1200	1000	0.02	under construction
8.0	1280[a]	1000	0.03[a]	operational
15.5	2170[a]	1000	0.05[a]	operational
35.5	2500	80	0.2	under construction

[a]Indicates measured value. Other values are theoretical. We have used $(\Delta T)_{rms} = 2T/\sqrt{B\tau}$ with $\tau = 10$ sec.

Output from the radiometers and various other information channels is fed into the U-490 digital computer for a certain amount of real-time processing concurrently with the pointing of the antenna. A sample of the high-speed printer output is shown in Fig. VIII-8.

3. Present Programs

Mapping of Radio Sources: At 15.5 Gc/sec, the antenna has a full width at half-power of 2.3 minutes of arc. This is sufficiently small to at least partially resolve many of

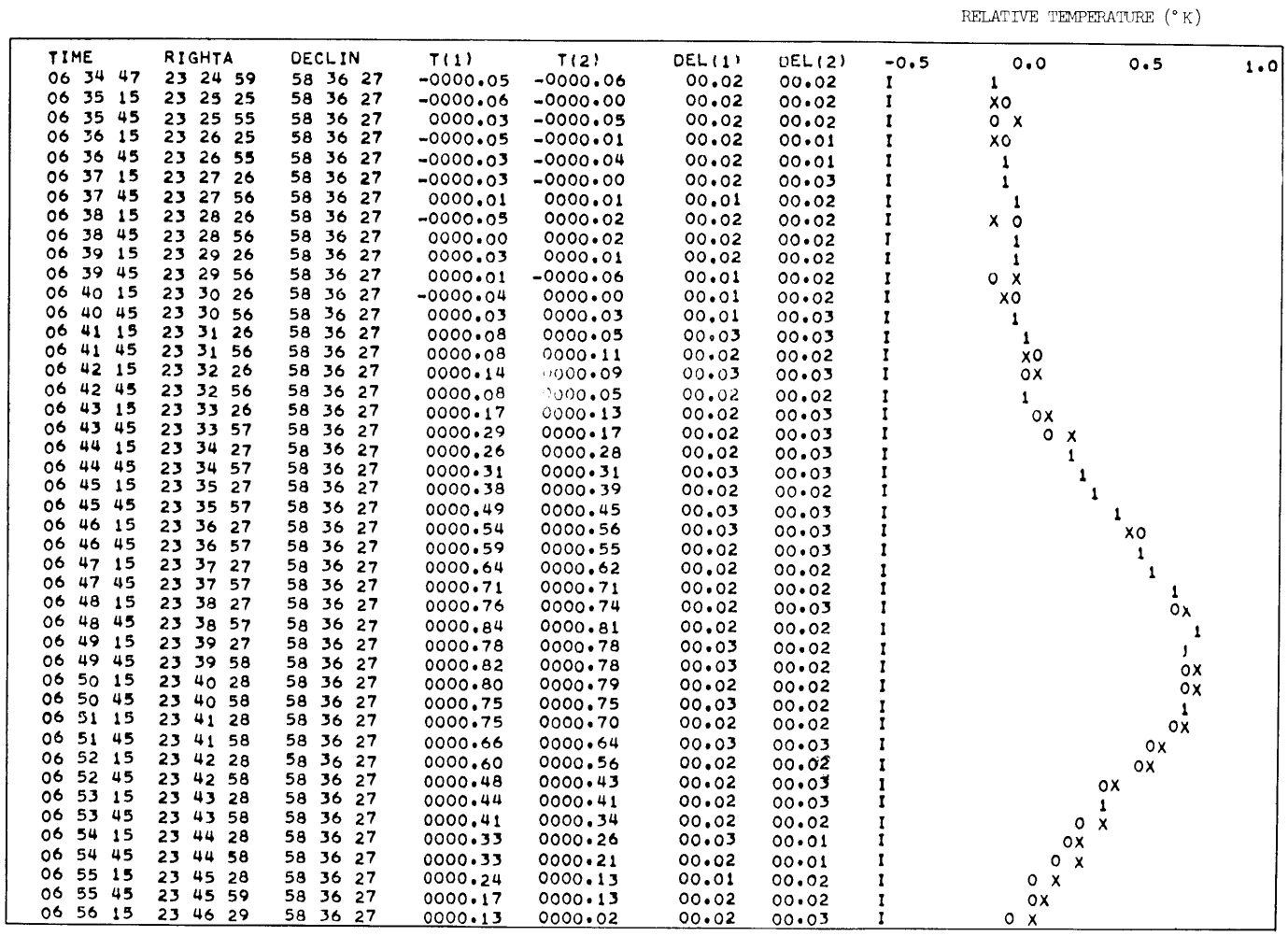

TIME	RIGHTA	DECLIN	T(1)	T(2)	DEL(1)	DEL(2)
06 34 47	23 24 59	58 36 27	-0000.05	-0000.06	00.02	00.02
06 35 15	23 25 25	58 36 27	-0000.06	-0000.00	00.02	00.02
06 35 45	23 25 55	58 36 27	0000.03	-0000.05	00.02	00.02
06 36 15	23 26 25	58 36 27	-0000.05	-0000.01	00.02	00.01
06 36 45	23 26 55	58 36 27	-0000.03	-0000.04	00.02	00.01
06 37 15	23 27 26	58 36 27	-0000.03	-0000.00	00.02	00.03
06 37 45	23 27 56	58 36 27	0000.01	0000.01	00.01	00.02
06 38 15	23 28 26	58 36 27	-0000.05	0000.02	00.02	00.02
06 38 45	23 28 56	58 36 27	0000.00	0000.02	00.02	00.02
06 39 15	23 29 26	58 36 27	0000.03	0000.01	00.02	00.02
06 39 45	23 29 56	58 36 27	0000.01	-0000.06	00.01	00.02
06 40 15	23 30 26	58 36 27	-0000.04	0000.00	00.01	00.02
06 40 45	23 30 56	58 36 27	0000.03	0000.03	00.01	00.03
06 41 15	23 31 26	58 36 27	0000.08	0000.05	00.03	00.03
06 41 45	23 31 56	58 36 27	0000.08	0000.11	00.02	00.02
06 42 15	23 32 26	58 36 27	0000.14	0000.09	00.03	00.03
06 42 45	23 32 56	58 36 27	0000.08	0000.05	00.02	00.02
06 43 15	23 33 26	58 36 27	0000.17	0000.13	00.02	00.03
06 43 45	23 33 57	58 36 27	0000.29	0000.17	00.02	00.03
06 44 15	23 34 27	58 36 27	0000.26	0000.28	00.02	00.03
06 44 45	23 34 57	58 36 27	0000.31	0000.31	00.03	00.03
06 45 15	23 35 27	58 36 27	0000.38	0000.39	00.02	00.02
06 45 45	23 35 57	58 36 27	0000.49	0000.45	00.03	00.03
06 46 15	23 36 27	58 36 27	0000.54	0000.56	00.03	00.03
06 46 45	23 36 57	58 36 27	0000.59	0000.55	00.02	00.03
06 47 15	23 37 27	58 36 27	0000.64	0000.62	00.02	00.02
06 47 45	23 37 57	58 36 27	0000.71	0000.71	00.02	00.02
06 48 15	23 38 27	58 36 27	0000.76	0000.74	00.02	00.03
06 48 45	23 38 57	58 36 27	0000.84	0000.81	00.02	00.02
06 49 15	23 39 27	58 36 27	0000.78	0000.78	00.03	00.02
06 49 45	23 39 58	58 36 27	0000.82	0000.78	00.03	00.02
06 50 15	23 40 28	58 36 27	0000.80	0000.79	00.02	00.02
06 50 45	23 40 58	58 36 27	0000.75	0000.75	00.03	00.02
06 51 15	23 41 28	58 36 27	0000.75	0000.70	00.02	00.02
06 51 45	23 41 58	58 36 27	0000.66	0000.64	00.03	00.03
06 52 15	23 42 28	58 36 27	0000.60	0000.56	00.02	00.02
06 52 45	23 42 58	58 36 27	0000.48	0000.43	00.02	00.03
06 53 15	23 43 28	58 36 27	0000.44	0000.41	00.02	00.03
06 53 45	23 43 58	58 36 27	0000.41	0000.34	00.02	00.02
06 54 15	23 44 28	58 36 27	0000.33	0000.26	00.03	00.01
06 54 45	23 44 58	58 36 27	0000.33	0000.21	00.02	00.01
06 55 15	23 45 28	58 36 27	0000.24	0000.13	00.01	00.02
06 55 45	23 45 59	58 36 27	0000.17	0000.13	00.02	00.02
06 56 15	23 46 29	58 36 27	0000.13	0000.02	00.02	00.03

Fig. III-8. Sample of the real-time data output from the U-490 computer.

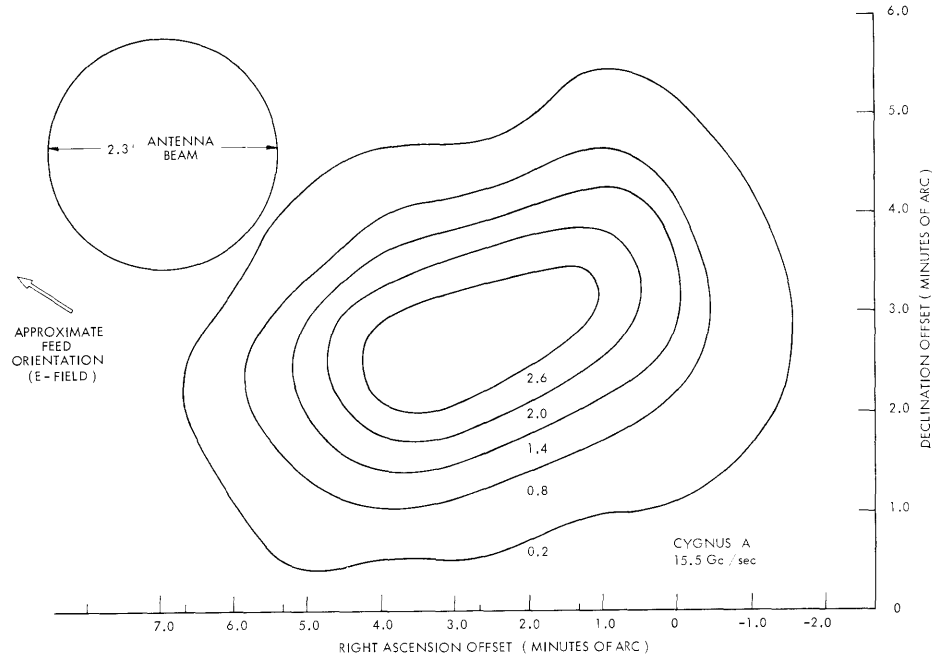

Fig. III-9. Contours of constant antenna temperature over the radio source Cygnus A.

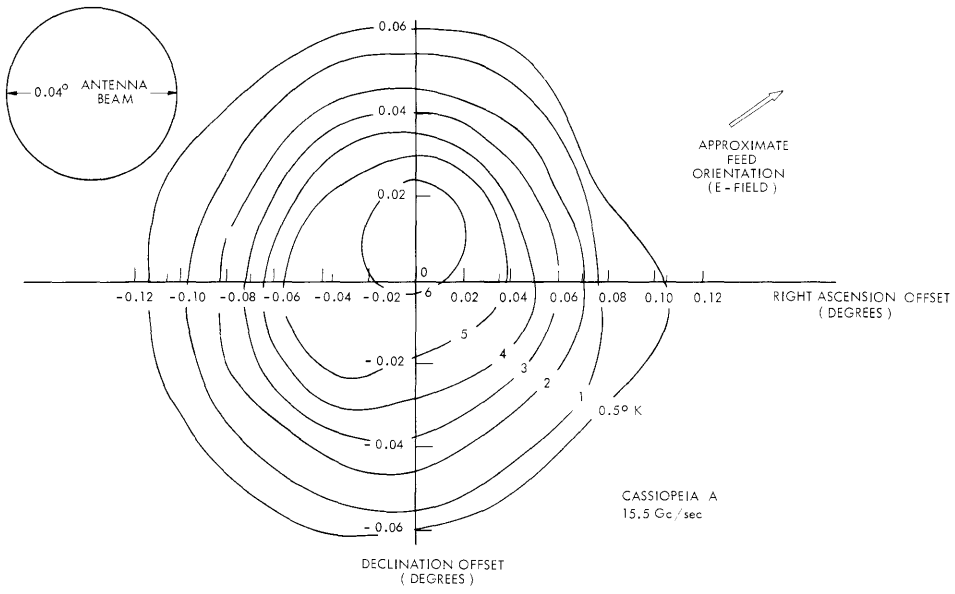

Fig. III-10. Contours of constant antenna temperature over the radio source Cassiopeia A.

the bright radio sources, and to map in some detail certain regions of extended continuum emission, such as Cygnus X and Centaurus A. From the lower frequency measurements, it has become evident that the geometrical shape of many radio sources seems to change slightly with frequency. Accordingly, we have begun to map some of the continuum sources at 15.5 Gc/sec.

The mapping proceeds as follows: The coordinates of a square grid of points covering the radio source are first calculated, with a spacing of one minute of arc used. The computer is then instructed to direct the antenna to the first point, which we call the "tie point", lying off the source in one corner of the grid of points, and the radiometer is then calibrated. The observations proceed by instructing the computer to direct the antenna to the various points on the grid at each point. The output of the synchronous detectors is integrated for 30 seconds, which results in a $(\Delta T)_{rms}$ of 0.02°K for each of the 500 Mc/sec channels. Of course, the antenna is tracking the source at the sidereal rate simultaneously. After every 5 or 6 points, the computer is instructed to return the antenna to the tie point. Thus at the conclusion of the observations, a graph of tie-point temperature against elevation can be drawn, and by interpolation the background radiation (which is due mainly to atmosphere) can be subtracted off at each observation point. A contour map of antenna temperature is then produced in the following manner. The data, corrected for background variations, is plotted as scans in right ascension, and also as scans in declination. A smooth curve is drawn through each set of points and the positions of the respective contour levels are transferred to the contour map. Joining of points of the same contour level produces the final result. Figure III-9 gives a preliminary map of Cygnus A, and Fig. III-10 shows the same for Cassiopeia A.

A computer program is being written by J. C. Henry of Lincoln Laboratory, M. I. T., to accomplish the curve fitting and contour plotting, using the 7094 computer along with the Calcomp plotter.

Radio flux: A program to measure the radio flux from sources at 8 and 15.5 Gc/sec is getting under way. A glance at publications shows that few radio sources have spectra measured beyond 3 Gc/sec. The versatility of the Haystack Antenna, and the sensitivity of the radiometric system make such measurements quite feasible. It has been suggested from a few measurements that beyond 5 Gc/sec many radio spectra depart widely from the simple power law. Measurements of spectra at higher frequencies will almost certainly affect the present models of radio sources. Therefore, the present program is planned to (i) extend the spectra of radio sources to short centimeter wavelengths, and (ii) search for sources such as planetary nebulae at these wavelengths.

R. J. Allen, A. H. Barrett, A. E. E. Rogers, S. H. Zisk

References

1. H. G. Weiss, "The Haystack Experimental Facility," Technical Report 365, Lincoln Laboratory, M. I. T., June 1965.

2. J. Ruze, "Interpretation of Recent Haystack Radiometric Measurements," Technical Memorandum 3L-302, Lincoln Laboratory, M. I. T., May 10, 1965.

3. M. L. Meeks and S. Weinreb, "An Initial Evaluation of Haystack," Technical Memorandum 31L-0013, Lincoln Laboratory, M. I. T., June 1965.